JMEPEG (2020) 29:1995–2005
https://doi.org/10.1007/s11665-020-04710-3

1059-9495/$19.00

Microstructure and Tribological Behavior of In Situ TiC-Ni(Si,Ti) Composites Elaborated from Ni and Ti_3SiC_2 Powders

Nabil Chiker, Abdessabour Benamor, Youcef Hadji, Adel Haddad, Maamar Hakem, Mohammed Azzaz, Tahar Sahraoui, and Mohamed Hadji

(Submitted October 5, 2019; in revised form January 31, 2020; published online March 9, 2020)

Herein, we study the effect of Ti_3SiC_2 on the microstructures and tribological properties of an in situ TiC reinforced Ni(Si, Ti) composites elaborated from Ni and Ti_3SiC_2 MAX phase powders against steel (100Cr6). Pressureless sintering at 1080 °C for 4 h of Ni and Ti_3SiC_2 powders was used to elaborate these composites with 10, 20 and 30 wt.% of Ti_3SiC_2. The microstructures of the composites were investigated by scanning electron microscopy (SEM), x-rays diffraction and Raman spectroscopy. Standard ball-on-disk friction wear tests under different applied loads were conducted on the composites surfaces at room temperature. For the three elaborated composites, Ti_3SiC_2 was totally decomposed and transformed to TiC phase, while the released Si and Ti atoms from Ti_3SiC_2 diffused into Ni matrix forming Ni(Si, Ti) solid solution. As compared with reference (Ni) sinter, the addition of 20 wt.% Ti_3SiC_2 in the Ni matrix improved the hardness by ~ 250%. The addition of Ti_3SiC_2 particles also had a beneficial effect on the tribological performance of these composites against steel. The worn surfaces of the elaborated composites under all applied loads are characterized by the presence of a lubricious Fe_3O_4-αFe_2O_3 tribofilms. The effect of chemical compositions and different applied loads on the wear mechanisms of the three elaborated composites is discussed.

Keywords In situ composites, MAX phase, microstructures, wear

1. Introduction

Nickel (Ni) is a highly versatile material that can alloy with most other metals, which give it the ability to be used in a wide variety of industries, such as automobile, aircraft gas turbines and its extensive use in energy and nuclear power markets. Besides its high versatility, its outstanding heat and corrosion resistance, good toughness and high tensile strength make it a popular choice as the matrix in metal matrix composites (MMCs). Many attempts were made in order to improve its wear resistance and anti-frictional properties by dispersing both hard and soft reinforcements. Ramesh and Seshadri (Ref 1, 2) showed that dispersing silicon nitride, fly ash and calcium fluoride in nickel matrix composites coatings on mild steel substrates, by sediment electro-co-deposition (SECD) technique, improved the wear properties of the coating. Cui et al. (Ref 3) studied the TiC particles composite coating produced with pure (Ti, C and Ni) powders by laser cladding technique on gray cast iron substrate. They found that both hardness and wear resistance after coating were significantly improved, which is attributed to the existence of in situ TiC in the laser-clad layer. Titanium carbide (TiC) is one of the widely used ceramics as reinforcement in composite materials (Ref 4-7); beside its good hardness (28-31 GPa), high modulus and high stability at elevated temperatures, TiC also provides a good wear resistance (Ref 8). By means of wear resistance, intermetallic compounds such nickel-based ones (Ni_3Si) also possess many attributes necessary for this property (high strength, high elastic modulus and good environmental stability). Niu et al. proved that Ni_3Si-based composites have an excellent wear resistance at ambient (Ref 9) and high temperature (Ref 10).

Few research works have focused on Ni-Si-Ti-C system to fabricate an in situ Ni_3Si and TiC particles reinforced MMCs. This composite system proved itself as a good wear resistant coating (Ref 11).

MAX phases are thermodynamically stable nanolaminates ceramics displaying unique properties (Ref 12, 13). With a general formula $M_{n+1}AX_n$ ($n = 1 - 3$) where M is an early transition metal, A is an element from groups IIIA or IVA in the periodic table, and X is C or N. Ti_3SiC_2 is the most characterized MAX phase, and ideal candidate for our project. MAX phases were considered as an expensive material until 2016, when Istomina et al. (Ref 14) have succeeded to reduce the cost of Ti_3SiC_2 MAX phase synthesis, through reduction in titanium dioxide (TiO_2) with silicon carbide (SiC) and elemental Si. They showed that the purity of Ti_3SiC_2 sample reached 96 wt.%. It is well established that the decomposition of MAX phases is triggered by the outward diffusion of A element that

Nabil Chiker, Abdessabour Benamor, Youcef Hadji, Adel Haddad, and **Tahar Sahraoui**, Laboratoire d'Etudes et Recherche en Technologie Industrielle, LERTI, Université BLIDA1, B.P 270, Route de Soumaa, Blida, Algeria; **Maamar Hakem**, Research Center in Industrial Technologies, CRTI, BP 64, Route de Dely Brahim, Chéraga, Algeria; and **Mohammed Azzaz**, Laboratoire des Sciences et de Génie des Matériaux (LSGM), Université des Sciences et de la Technologie Houari Boumediene (USTHB), BP 32, El-Alia, Bab-Ezzouar 16111 Alger, Algeria; and **Mohamed Hadji**, Laboratoire d'Etudes et Recherche en Technologie Industrielle, LERTI, Universite BLIDA1, B.P 270, Route de Soumaa, Blida, Algeria; and Research Center in Industrial Technologies, CRTI, BP 64, Route de Dely Brahim, Chéraga, Algeria. Contact e-mail: nabilc21@gmail.com.

causes the formation of transition metal carbide or nitride (Ref 15, 16). The released A element (Si) in our case can react with the surrounding Ni matrix to form a Ni solid solution and dispersed Ni_3Si intermetallic. However, achieving the formation of a significant amount of Ni_3Si is challenging due to insufficient content of A element in Ti_3SiC_2.

Recently, in situ formation of TiC, Ni(Si, Ti) solid solution through Ti_3SiC_2 MAX phase decomposition in reinforced Ni matrix was successfully synthesized (Ref 17). This new composite system derived from reactive sintering approved its efficiency by its outstanding mechanical properties. As far as we are aware, to date no work has been carried out on characterizing their tribological behavior. Thus, the aim of our work is initially to fabricate an in situ TiC reinforced Ni metal matrix via powder metallurgy route, starting with Ti_3SiC_2 MAX phase and pure nickel as reactive powders. The effect of Ti_3SiC_2 contents on phase composition, microstructure, hardness and wear resistance is reported.

2. Experimental Details

2.1 Raw Materials

Ti_3SiC_2 powder (available commercially under the name Maxthal312; Sandvik Heating Technology, Sweden) and nickel

Table 1 Powder mixtures and the density of the different elaborated composites

Sample	Nickel, wt.%	Maxthal312, wt.%	Density, g/cm^3
Ni	100	…	8.42 ± 0.21
NTSC10	90	10	6.21 ± 0.26
NTSC20	80	20	5.73 ± 0.19
NTSC30	70	30	5.54 ± 0.36

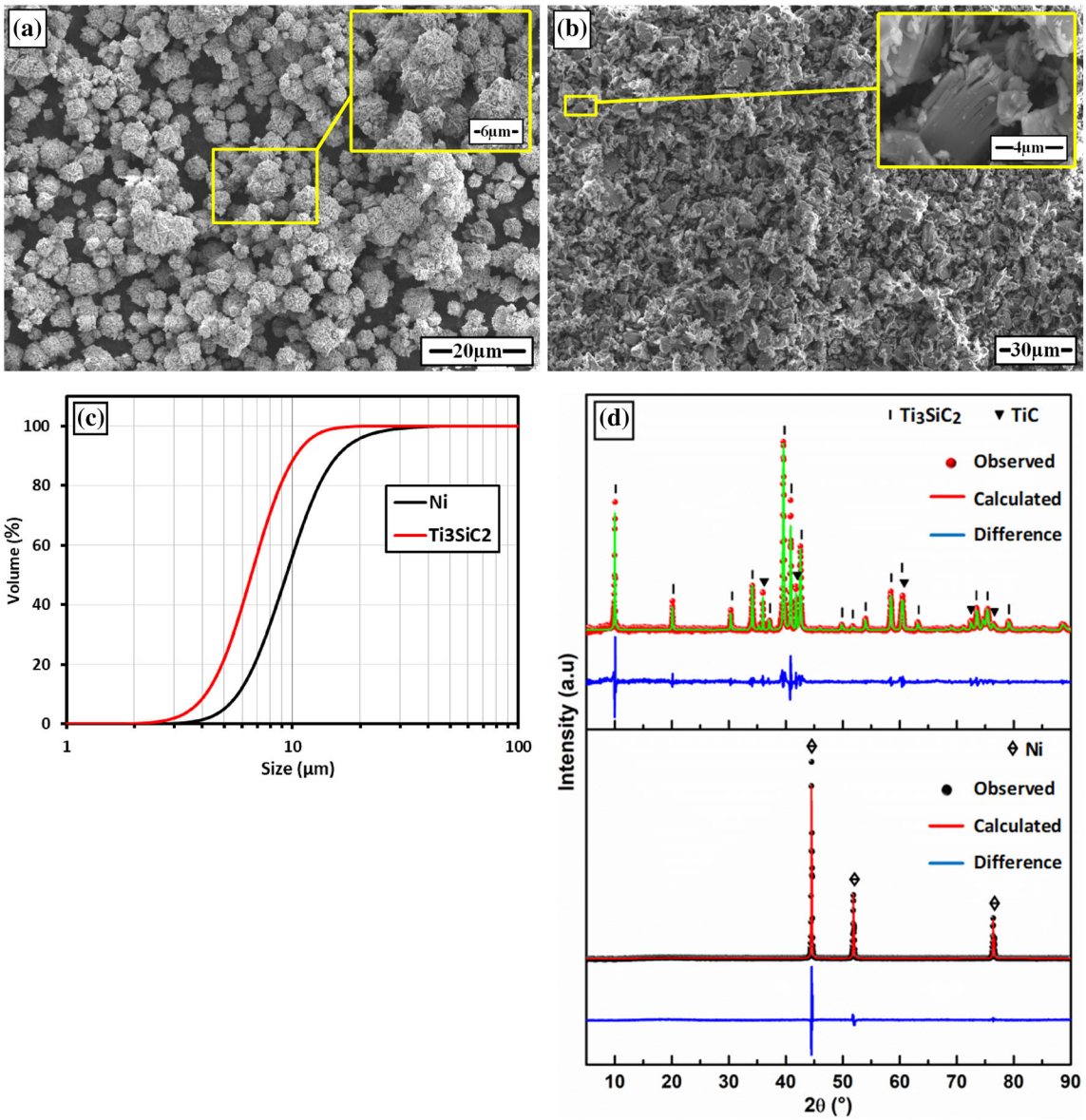

Fig. 1 SEM micrographs of the starting materials, (a) Ni powder; (b) Ti_3SiC_2 powder; (c) particles size distribution of Ni and Ti_3SiC_2 powders; (d) x-rays diffraction patterns of starting materials. Bottom pattern (black) shows diffractogram of Nickel powder. Top pattern (red) is that of Ti_3SiC_2 powder

(Ni) powder (Aldrich chemical company. Inc) were used. Laser scattering particle size analyzer (HORIBA LA-960) was used to test the particles size distribution of raw powders.

2.2 Samples Preparation

Ni/Ti_3SiC_2 composites were fabricated, by preparing a powder mixtures of Ni with 10, 20 and 30 wt.% of Ti_3SiC_2 powder (see Table 1). All the compositions were dry milled for 15 min in a PM 400 planetary mill (RETSCH, Germany) using zirconia balls, with ball-to-powder ratio of 5:1 at a rotary speed of 250 r/min. The mixed powders were then cold pressed in a $\sim$ 16 mm stainless steel die with a uniaxial compressive stress $\sim$ 560 MPa for 15 min. For comparison, pure Ni sample was also prepared under similar conditions. The composites were sintered at 1080 °C for 4 h in a controlled atmosphere furnace, under Ar environment. Density and open porosity of the elaborated samples were measured by Archimedes' method in water. The phase composition of the starting powders and the elaborated composites was determined using an x-ray diffractometer (PANalytical, X'Pert3 Powder) with Cu Kα radiation (1.542 Å); 2θ ranged from 5° to 80° with a 0.02° step size and 1 s step time. Rietveld analysis was performed using Material Analysis by Diffraction/Reflectivity (MAUD) software (Ref 18, 19). The phase fractions and the lattice parameters were refined using the least-squares refinement implemented in MAUD. Samples for SEM were prepared by mechanical grinding gradually using (280-4000) grade SiC sandpaper and then ultrasonically cleaned in ethanol for 5 min to remove any residual SiC particles from grinding on the samples surfaces. Backscattered electron (BSE) and secondary electron (SE) images were obtained using SEM, (Quanta 650; FEI Netherlands), equipped with an energy-dispersive x-ray spectrometer (EDS), (Brucker X Flash 6/10). The conditions used for SEM images were: (high vacuum, 10 mm working distance, 2 µA beam current intensity, spot size 4 and an accelerating voltage of 20 kV). For EDS analysis, the detector window was 3.3 µm Al; the acquisition time for each analysis was 120 s, with an energy resolution of 129 eV (Mn Kα FWHM). Note that standardless-based semi-quantitative analysis through peak-to-background model and subsequent ZAF-correction (P/B-ZAF) was automatically performed; however, all C and O concentrations reported herein have to be taken with a grain of salt given the known inability of EDS to correctly quantify C and O−. The Raman spectra on the wear tracks were recorded using a spectrophotometer (Horiba LabRAM HR Evolution, Japan) equipped with an Ar + ion laser operating at a wavelength of 633 nm, with an incident power of 17 mW. In these measurements, 10% laser power was used for 10 s of exposure time.

Table 2 Summary of weight fractions and lattice parameters of Ni, Ti_3SiC_2 and TiC phases obtained from Rietveld analysis of XRD patterns of the Ni and Maxthal312 powders

		Lattice parameter	
Phase	**wt.%**	***c*, nm**	***a* = *b*, nm**
Nickel Powder Ni	99.99	a = 0.3524	
Maxthal312 Powder Ti_3SiC_2	87	1.7660	0.3065
TiC	13	a = 0.4319	

The hardness of the samples was tested by using a Vickers hardness indenter (INOVATEST NEXUS 4300) with an indentation load of 10 Kgf for 15 s. An average of 5 readings for each composition is reported in the text. The tribological properties were determined by a ball-on-disk method using a micro-mechanical property test system (CSM Tribometer, Switzerland). All wear tests were performed in an open atmosphere, without a lubricant, by pressing a 6 mm diameter steel ball (100Cr6, Hv $\sim$ 8GPa) on to rotating composites disks. The applied normal forces (F_N) were 2, 6 and 10 N, at a

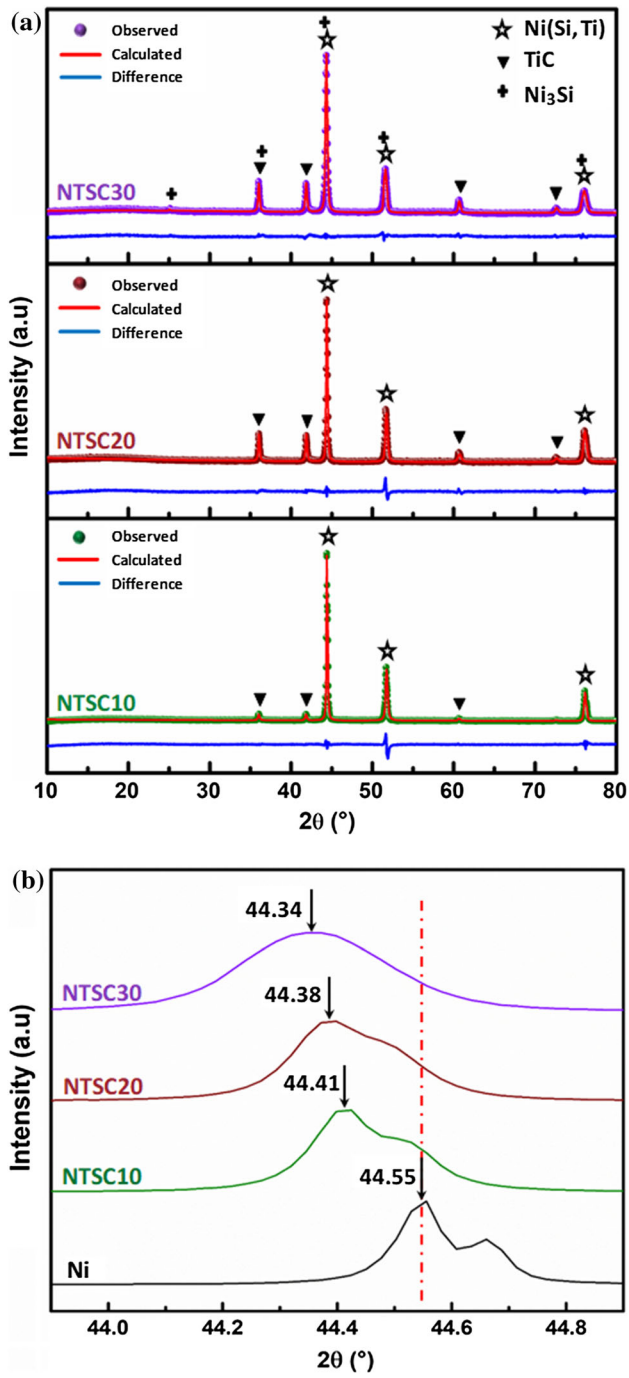

Fig. 2 (a) Rietveld refined x-ray diffraction patterns of NTSC10 (green line), NTSC20 (brown line) and NTSC30 (violet line). (b) Enlarged XRD patterns of (a), between 43.8° and 44.9° (for comparison, pure Ni pattern is also shown)

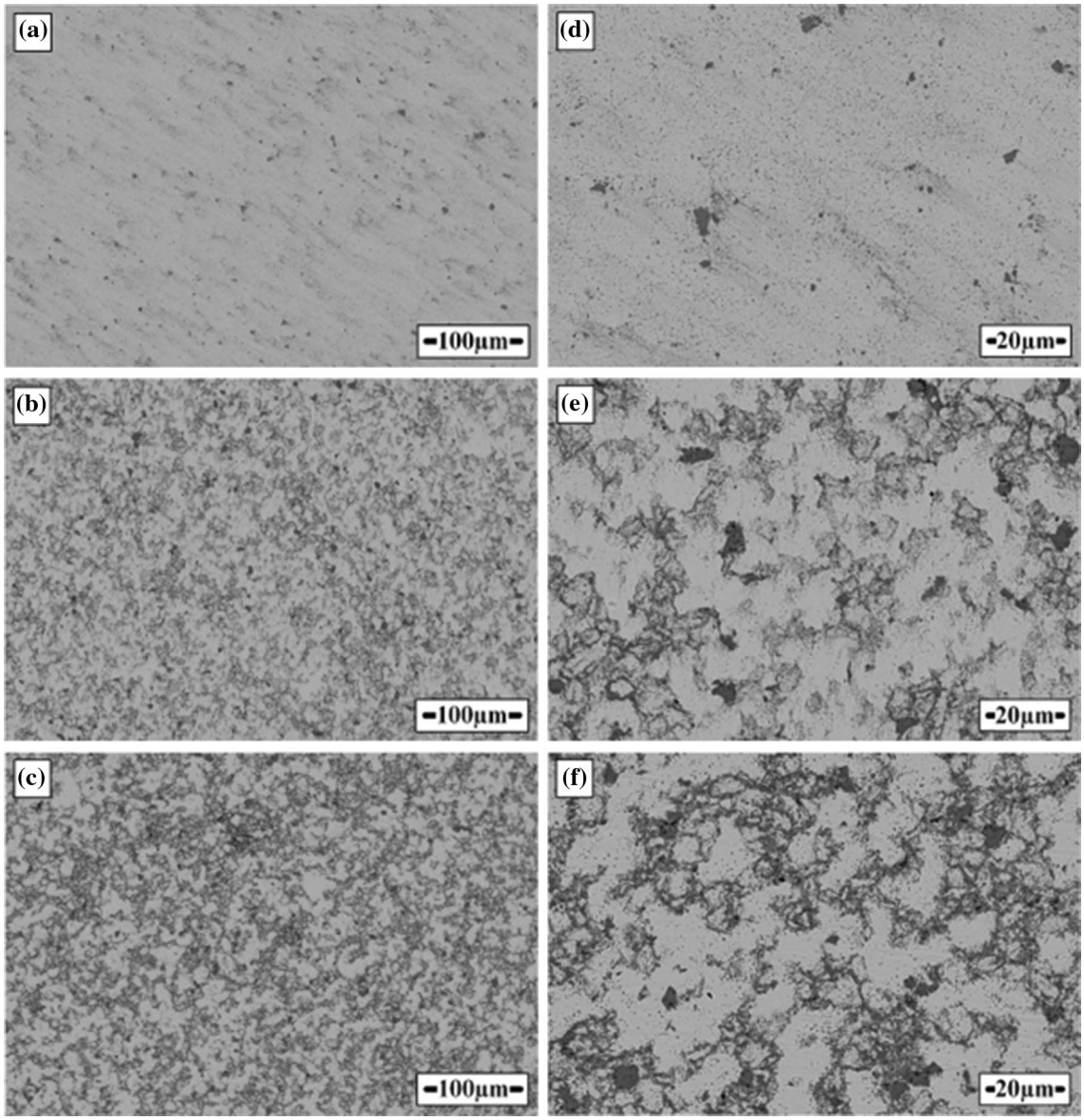

Fig. 3 SEM images of NTSC composites top surfaces: (a) NTSC10, (b) NTSC20, (c) NTSC30; (d), (e) and (f) are higher magnification of (a), (b) and (c), respectively

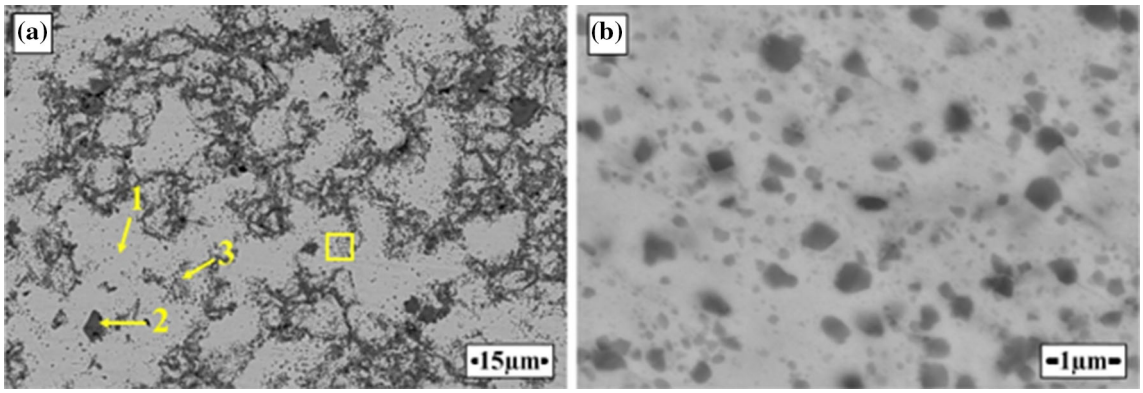

Fig. 4 SEM images of (a) NTSC30 composite top surface, (b) a higher magnification of the area represented by a rectangle in (a)

relative sliding speed of 55 mm/s. The tribometer was programmed to stop the test when μ were higher than 1.2 or the sliding distance was > than 150 m, whichever came first. An average of the final 20 meters data points of the friction coefficient (μ) was used to calculate steady state friction coefficient (μ). The arithmetic roughness Ra (Ra < 0.05 μm) and the 2D profiles of the samples surface were measured using a 2D profilometer (Tribotechnic, France). Specific wear rates (WR's) were calculated by initially finding the surface area of the 2D plots which is provided by the computer and multiplying it with the track circumference, i.e., 2πr, where r symbolizes the track radius, to calculate the wear volume (V). The wear volume is then divided by the applied normal load (F_N) and distance (d) travelled by the ball as shown in Eq. 1:

$$\mathrm{WR} = V/(F_N \cdot d) \quad \text{(Eq 1)}$$

3. Results and Discussion

3.1 SEM and XRD Results of the Starting Powders

SEM micrographs of Ni and Ti_3SiC_2 powders are shown in Fig. 1. Ni powder is composed of discrete, spiky, needle-like particles, as shown in Fig. 1(a). This unique feature makes it perfect for powder metallurgy applications. Figure 1(b) shows Ti_3SiC_2 particles having an irregular shape. The insets in Fig. 1(b) illustrate the characteristic of Ti_3SiC_2 nano-laminated structure. Figure 1(c) represents the particle size distribution of each powder; it indicates that Ni and Ti_3SiC_2 powders have ~ 4-30 μm and ~ 2.5-15 μm range, respectively.

Table 2 summarizes the Rietveld analysis results of the Ni and Ti_3SiC_2 powders. The refined XRD diffraction patterns of the starting materials are shown in Fig. 1(d). The Ti_3SiC_2 (Maxthal312) powder (top panel in Fig. 1(c)) indicates the presence of two phases with approximately ~ 87 wt.% Ti_3SiC_2 and ~ 13 wt.% TiC. The latter originates from powder synthesis and often found as an impurity phase in commercially available Ti_3SiC_2 (Ref 20). The sharp diffraction peaks in the patterns indicate that all powders (Ti_3SiC_2 and Ni) are highly crystallized. The lattice parameters obtained are in good agreement with those reported in the literature for these phases.

Table 3 Summary of EDS results in at.% obtained from the various regions labeled in Fig. 4(a)

Spot	Ni	Ti	Si	C	Figures
1	90 ± 3	4 ± 4	6 ± 10	…	Figure 4(a)
2	2 ± 7	54 ± 5	…	44 ± 10	Figure 4(a)
3	53 ± 10	19 ± 5	3 ± 5	25 ± 13	Figure 4(a)

3.1.1 Microstructures of the Elaborated Composites from Ni and Ti_3SiC_2 Powders. Figure 2(a) shows the refined x-ray diffraction patterns of the Ni/Ti_3SiC_2 elaborated (cold pressed and sintered at 1080 °C) composites with different amounts of Ti_3SiC_2. They are referred to as NTSC10, NTSC20 and NTSC30 for composites synthesized with 10, 20 and 30 wt.% of Ti_3SiC_2, respectively. No Ti_3SiC_2 peaks have been detected. From the x-ray diffraction patterns, the NTSC10 and NTSC20 composites are composed (bottom and middle patterns, respectively) of TiC and Ni(Si, Ti) solid solution. This indicates that a strong reaction between Ni and Ti_3SiC_2 particles occurred at 1080 °C, which led to a total decomposition of Ti_3SiC_2 MAX phase. When Ni comes into contact with Ti_3SiC_2 particles, the good affinity between Ni and Si induces the de-intercalation of Si from Ti_3SiC_2 phase along the basal planes, leading to the formation of TiC, while the released Si and Ti atoms from Ti_3SiC_2 diffuse into Ni matrix forming Ni(Si, Ti) solid solution as illustrated in Eq. (2) (Ref 17).

$$Ti_3SiC_2 + Ni \rightarrow TiC + Ni(Si, Ti) \quad \text{(Eq 2)}$$

From the diffraction pattern of the NTSC30 composite (top pattern), besides TiC and Ni(Si, Ti) a third phase was identified (Ni_3Si intermetallic). It is difficult to distinguish between the XRD peaks of Ni and Ni_3Si phases because they possess the same cubic structure, with close lattice constant 'a' being

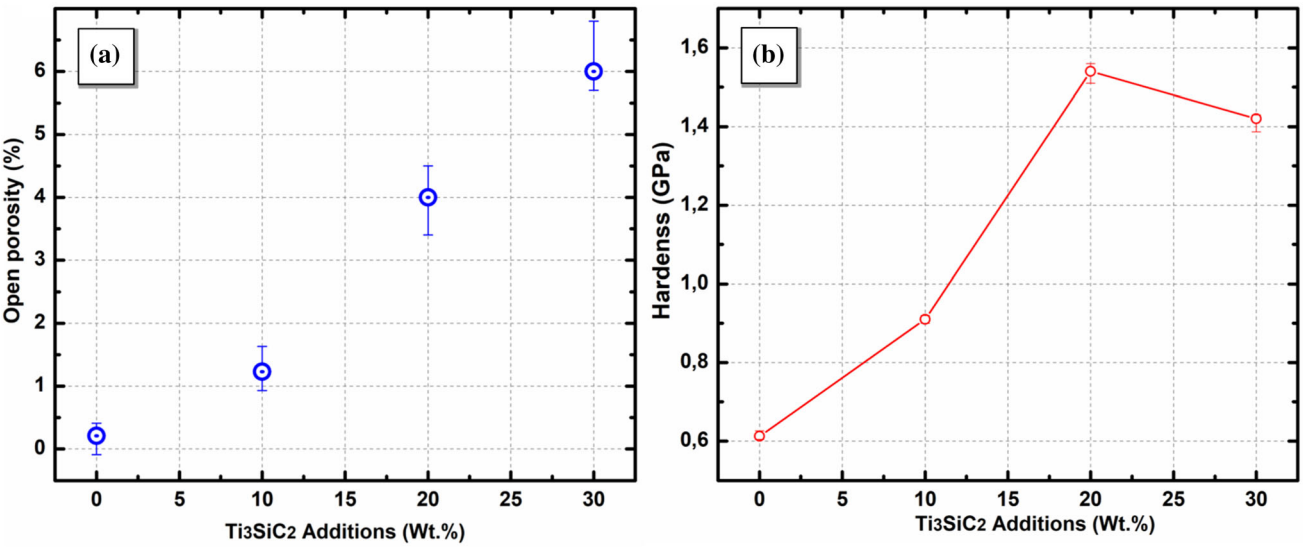

Fig. 5 Plots of (a) open porosity vs. wt.% of Ti_3SiC_2 and (b) Vickers hardness vs. wt.% of Ti_3SiC_2 addition in Ni matrix

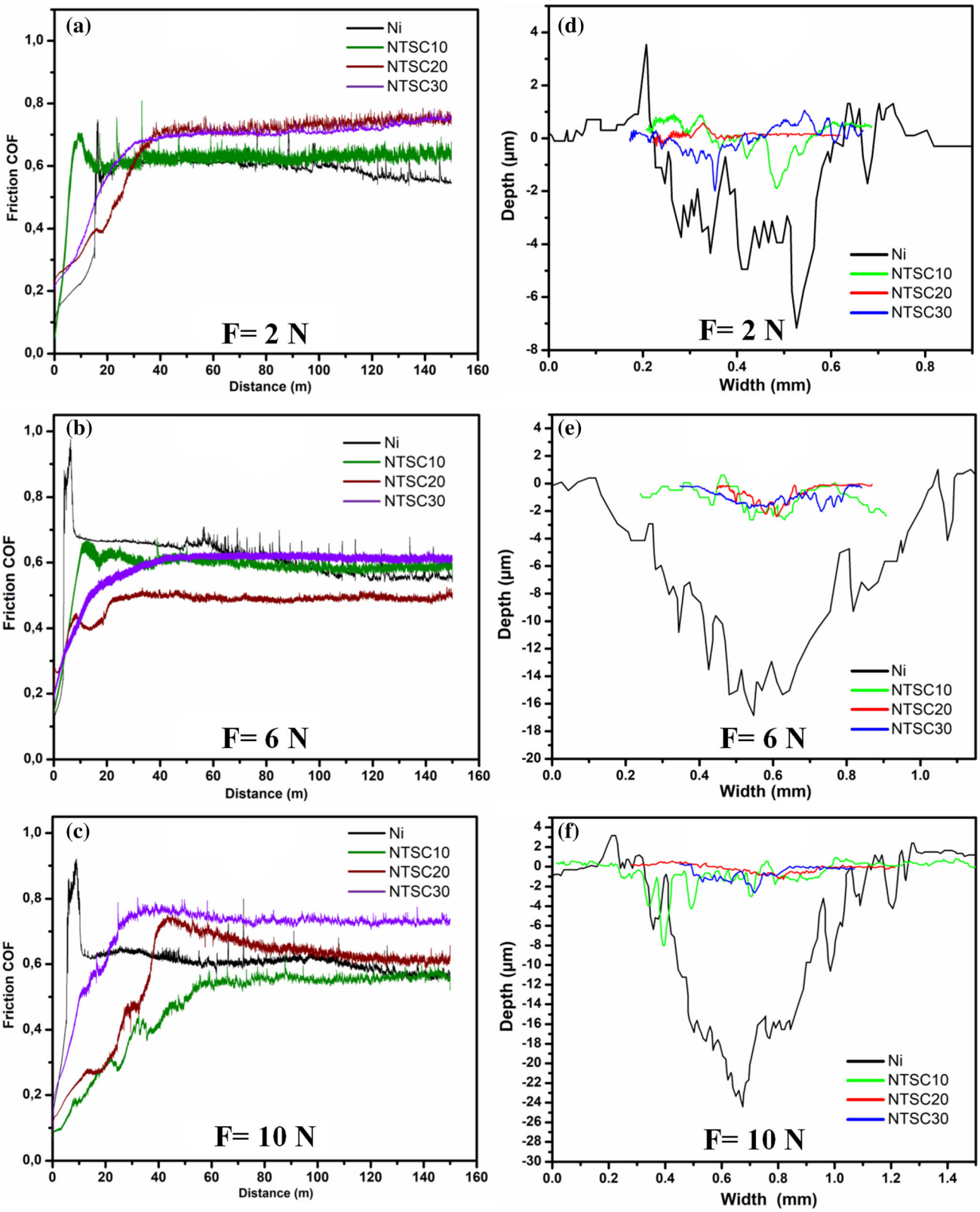

Fig. 6 Variation of friction COF (μ) with sliding distance of the NTSC composites/100Cr6 steel couple at (a) 2 N, (b) 6 N and (c) 10 N. (d), (e) and (f) represent the 2D profiles of all wear tracks after tribology tests for NTSC composites under 2 N, 6 N and 10 N, respectively

0.3524 nm (Ni) and 0.3510 nm (Ni_3Si). A number of previous studies on Ni-Si alloys have shown overlapping Ni and Ni_3Si XRD peaks (Ref 21, 22). Here, the presence of Ni_3Si phase can only be confirmed according to the presence of the unique, but very weak, characteristic peak corresponding to the (100) plane at 25.11°.

It is observed that the peak of Ni between 44° and 45° shifts from 44.55° to lower angles with the increase of Ti_3SiC_2 content as shown in Fig. 2(b). According to Bragg's law, it indicates an increase of lattice parameter. The measured lattice constants of Ni(Si, Ti) solid solution of NTSC10, NTSC20 and NTSC30 composites are 0.3531, 0.3534 and 0.3537 nm, respectively. Based on the reported data, we attribute the shift of Ni peaks and the increase in lattice constants to the formation of Ni(Si, Ti) solid solution.

Backscattered electron images of NTSC composites are shown in Fig. 3. A good distribution of Ti_3SiC_2 particles inside the Ni matrix having an irregular shape has been observed. Figure 4(b) shows a high magnification of the rectangle marked in Fig. 4(a) of the NTSC30 composite. It is characterized by a nanometric size particles with different contrasts (light and dark gray) embedded in the Ni matrix. These particles probably represent the Ni_3Si intermetallic and/or a refined TiC particles. It has been reported that the in situ formation of particles generates a much smaller size of the reinforcement particles and cleaner (particle/matrix) interfaces (Ref 23).

The amount of constituent elements in different regions determined by EDS from Fig. 4(a) is summarized in Table 3). For NTSC30 composite, the light gray region (point 1) represents Ni matrix in which small amount of Si and traces of Ti has entered the crystal structure of Ni forming the Ni(Si, Ti) solid solution. The dark gray area (point 2) is consistent with titanium carbide (TiC); and point 3 represents probably a mixture of different phases (TiC, Ni(Si, Ti) solid solution and Ni_3Si intermetallic).

3.2 Open Porosity and Hardness Measurements of the Elaborated Samples

Figure 5(a) shows the open porosity variation in NTSC composites as a function of reactive Ti_3SiC_2 volume fractions. It indicates that porosity varies linearly with the increase in Ti_3SiC_2 content. This result denotes that pressureless sintering of NTSC composites becomes difficult as the concentration of Ti_3SiC_2 in the Ni matrix increases. Same phenomena have been observed by Gupta et al. (Ref 24), in their pressureless-sintered Al/Ti_3SiC_2 composites.

Hardness studies showed that the three NTSC composites exhibited higher hardness than pure nickel, as shown in Fig. 5(b). The hardness improvement of these composites can be attributed to the high hardness of the TiC particles (resulted from the total decomposition of Ti_3SiC_2 phase), the Ni(Si, Ti) solid solution formation and the good adhesion between the latters. The NTSC composites hardness increases as a function of Ti_3SiC_2 content up to 20 wt.%. However, a decrease in hardness was observed from 20 to 30 wt.% of Ti_3SiC_2. This can be attributed to the high porosity displayed by this composite as shown in Fig. 5(a).

3.3 Wear and Friction Behavior of the Elaborated Samples

Figure 6(a), (b), (c) shows the relationship between μ and the sliding distance, up to 150 m under different applied loads for Ni and NTSC composites disks. It can be observed that the friction coefficients (μ) curves exhibit fluctuations that change from a composite to another. This could be attributed to the intense cohesive contact between the steel ball and the nickel matrix (Ref 25). From Fig. 6(a), (b), (c), the friction coefficient (μ) of Ni/steel pair is approximately ∼ 0.55. However, the μ's of the three NTSC composites varies in a range from ∼ 0.50 to ∼ 0.75. It indicates that the μ values of these composites are not very sensitive to in situ TiC amount, under similar testing conditions. The low μ observed for NTSC20 composite (0.50), under the load of 6 N, is may be due to a more homogeneous and smoother tribofilm formation during the sliding process.

Figure 6(d), (e), (f) shows the 2D profiles of all wear tracks of pure Ni and of the three elaborated composites. As compared with pure Ni, it can be seen that the wear tracks depths of NTSC composites (under different applied loads) have decreased dramatically. The effect of load on wear rates (WR's) of Ni and NTSC composites is shown in Fig. 7. An improvement in wear resistance is clearly seen, the WR's of the composites is way smaller than those of pure Ni under all normal loads. The drastic reduction in WR can be attributed to the following reasons: (a) the enhanced hardness of the composites (Ref 26); (b) the quality of bond between the matrix and the particles (Ref 26, 27); and (c) the great reduction in the direct metal-to-metal contact between the composite surface and the ball during sliding (Ref 28).

The WR's of the NTSC composites decreases with increase in the amount of the reinforcing particles, as shown in Fig. 7. The smallest WR's recorded values are those of NTSC20 and NTSC30 composites. This is due to the higher hardness displayed by these composites (Fig. 5b). The incorporation of in situ hard particles into Ni matrix provides an irrefutable stress transferring. Since in situ method procures a good bonding between the matrix and reinforcements, particles decohesion was avoided, and the loading stresses under sliding action were well transferred.

Panoramic views of the wear tracks generated under the different applied loads for NTSC10 and NTSC30 composites are shown in Fig. 8. All the wear tracks shown are characterized by the presence of a tribofilms. Table 4 summarizes the results of the EDS analysis of the worn surfaces for NTSC10 and NTSC30 composites. For NTSC30, the composition in spot 4 (tribofilm) showed the presence of iron (Fe ∼ 32 at.%) and oxygen (O ∼ 63 at.%); this result is a proof that an important material transfer from the steel ball to the surface of the composite occurred during the test. Note that all the formed tribofilms have almost the same composition. Similar O-

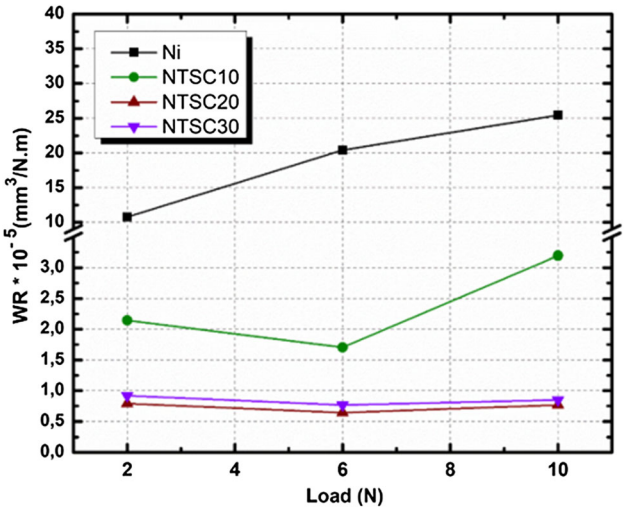

Fig. 7 The calculated wear rate (WR) values under the different applied loads for pure Ni and NTSC composites

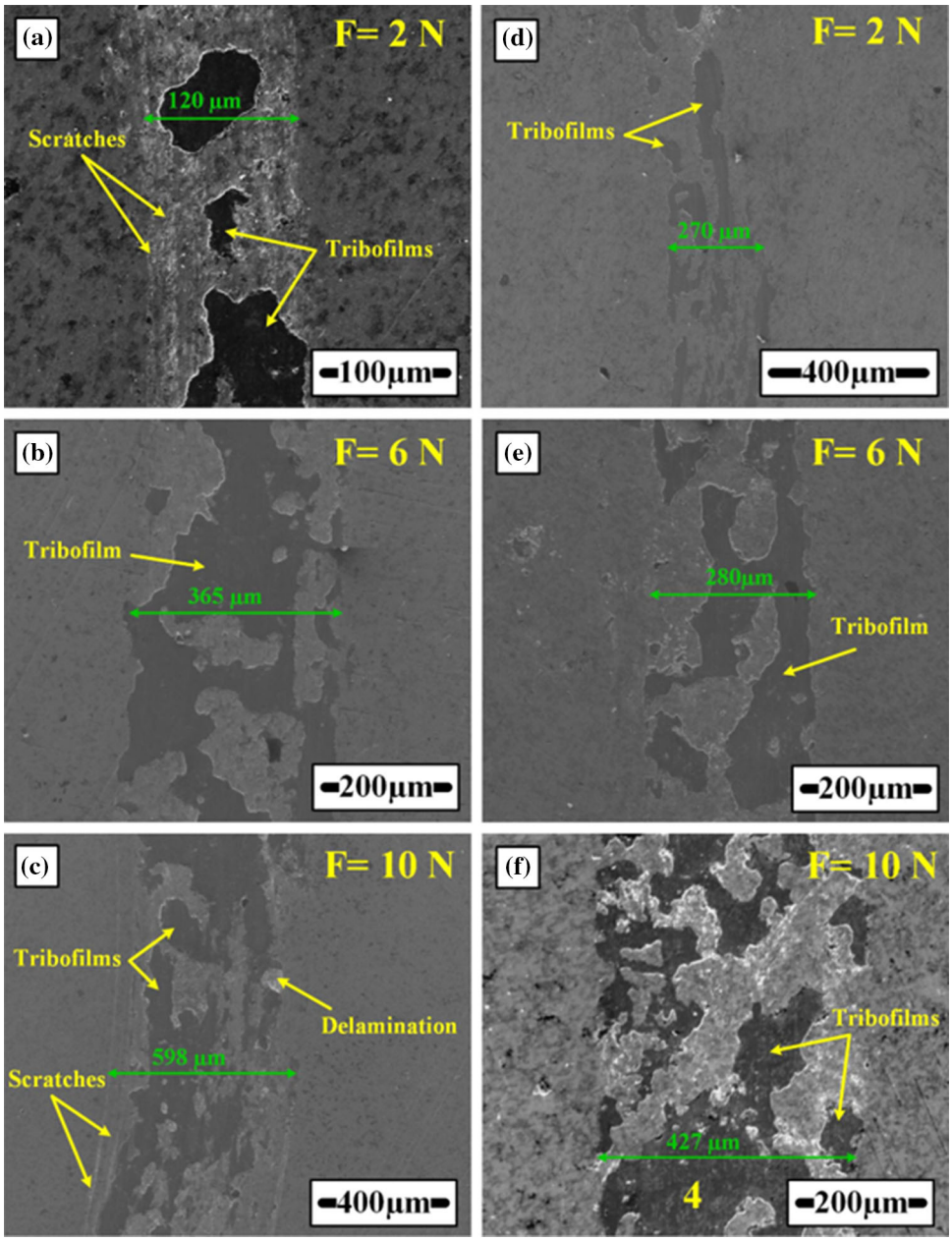

Fig. 8 SEM of the wear tracks of NTSC10 (a-c) and NTSC30 (d-f) under the different applied loads

Table 4 Summary of EDS results in at.% obtained from the various regions labeled in Fig. 8(a) and 11

Spot	Fe	O	Ni	Ti	Si	C	Figures
4	33 ± 5	63 ± 10	…	…	…	4 ± 3	Figure 8(f)
5	10 ± 2	36 ± 6	30 ± 5	2 ± 1	1 ± 3	21 ± 3	Figure 11

containing tribofilms have been reported in prior studies on dry-sliding of TiC and TiCN-Ni cermet systems (Ref 29, 30).

Figure 9 shows the Raman spectrum of the tribofilm formed on NTSC30 composite surface under 10 N load. It shows the presence of five bands (at ~ 301, ~ 388, ~ 471, ~ 530 and 669 cm^{-1}) that corresponds to Fe_3O_4 (Magnetite) oxide. These results are consistent with previously Raman studies on magnetite (Ref 31-33). Fe_3O_4 is known to have a lubricating property and is used as solid lubricant in many applications (Ref 34, 35). Additional weak bands at ~ 220 and ~ 410 cm^{-1}, and a broad one at ~ 1339 cm^{-1} were also found (Fig. 9). The latter belongs to the characteristic signature of α-Fe_2O_3 (Hematite) (Ref 31, 33). Hematite is also believed to have a lubricious property (Ref 36).

When we examine the wear tracks of the NTSC10 composite from Fig. 8(a), (b), (c), away from the tribofilm, it

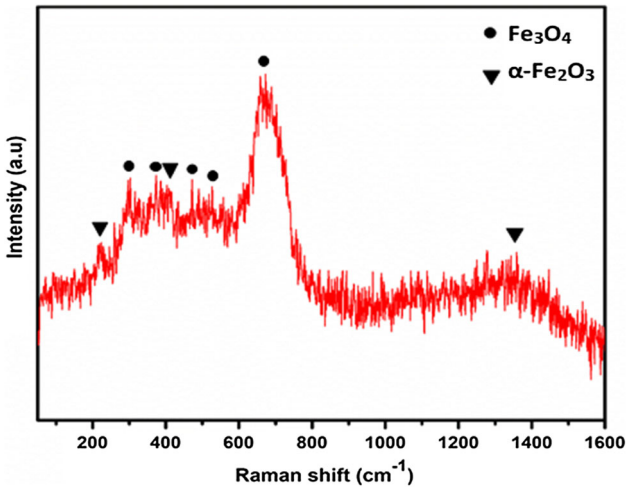

Fig. 9 Raman spectra of the formed tribofilm on NTSC30 composite surface under 10 N load

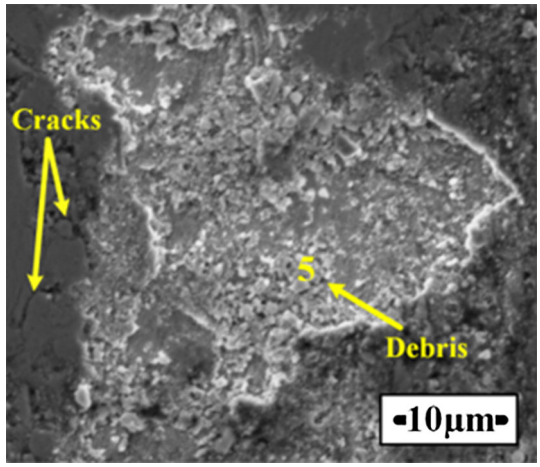

Fig. 11 A higher magnification of a delamination shown in Fig. 8 (wear track of NTSC10 under 10 N)

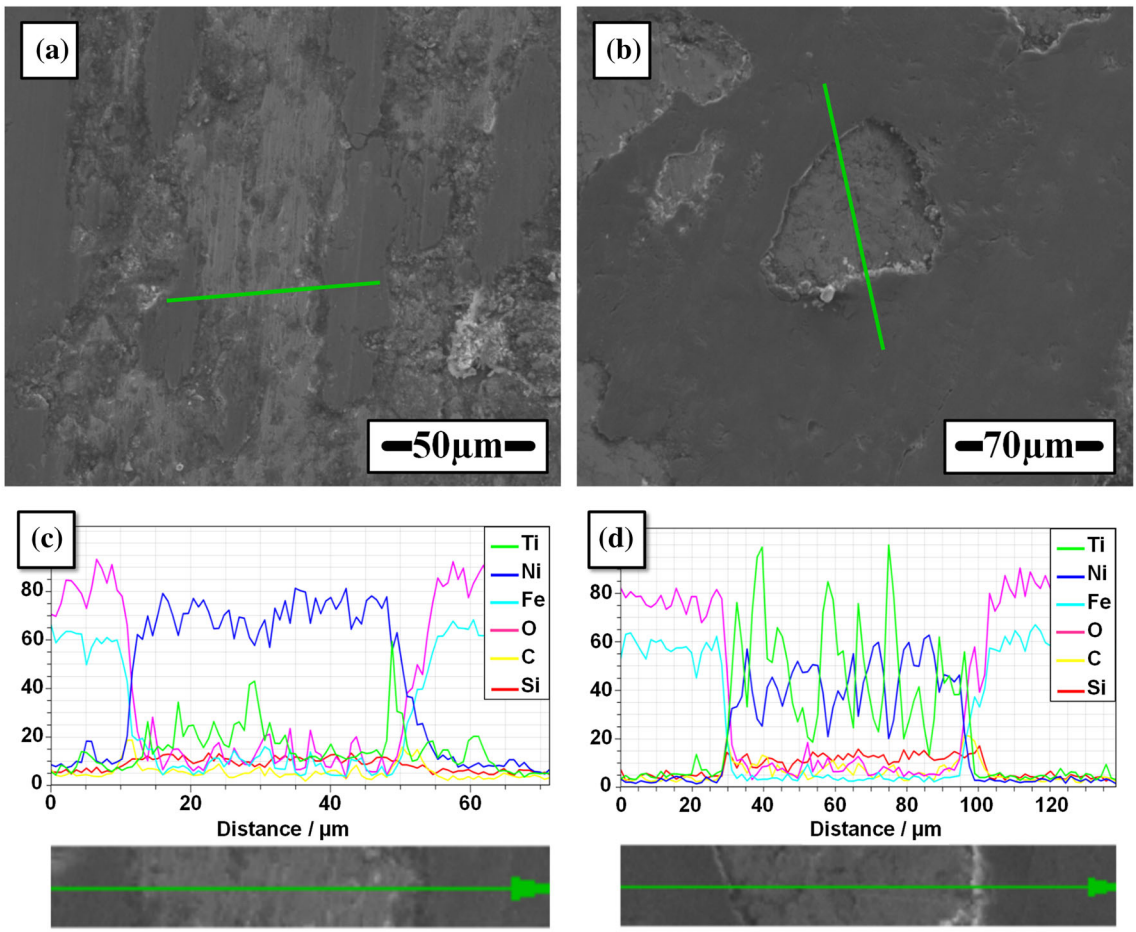

Fig. 10 SEM of the wear tracks of: (a) NTSC10 and (b) NTSC30 composites under 10 N load; (c) and (d) are the EDS line scans represented in (a) and (b), respectively

shows scratches and plastic deformation marks. The reason of that could be probably due to the low content of hard particles in this composite, which is dominated by a ductile Ni matrix. On the other hand, NTSC30 composite contains more hard particles that can reduce the contact area between the steel ball and the composite substrate. Several research works showed that, with increase in reinforcement ratio in a metallic–matrix, the amount of plastic deformation reduces (Ref 37-39). For

more investigation, higher SEM magnifications images of the wear tracks obtained under 10 N load of NTSC10 and NTSC30 composites are shown in Fig. 10(a), (b), respectively. The green lines represent the EDS line scans. The elemental compositions along those lines are shown in Fig. 10(c), (d). For NTSC10 (Fig. 10c), it is clear that Zone I (tribofilm) is comprised of Fe and O elements, which represent certainly the iron oxides (Fe_3O_4 and α-Fe_2O_3), as was determined by Raman spectroscopy; in Zone II, high Ni and small Ti signals were observed. It refers to the composition of the composite. In the same zone (Zone II), also a weak signal of oxygen is observed, which give a sign that a tribo-oxidation occurred in this area between the composite elements and O during friction. Zone III has the same characteristics as Zone I. The elemental composition along the line represented in Fig. 10d (wear track of NTSC30 under 10 N load) indicates the presence of Fe and O at the areas covered with a tribofilm (Zone I and III), while only Ni, Ti and traces of Si are present at the uncovered composite surface (Zone II), indicating that this composite is less affected.

The wear track of NTSC10 composite under 10 N load (Fig. 8c) reveals some areas of failures, which were not observed in NTSC30 composite (Fig. 8f). A higher magnification of one of those areas shows a delamination of the formed tribofilm (Fig. 11). According to EDS analysis (Table 4), the entrapped debris inside the delamination (spot 5) has a composition of (Ni $\sim$ 30 at.%, O $\sim$ 36 at.%, Fe $\sim$ 10 at.%, C $\sim$ 21 at.%, Ti $\sim$ 2 at.% and Si $\sim$ 1 at.%), indicating that a tribo-mixing between the elements of the detached tribofilm and the composite surface occurred. From this result, we can conclude that adhesion process (that causes the delamination of the tribofilm) is probably detaching out some areas of the NTSC10 composite located beneath the tribofilm surface, causing more material loss.

From the above results, we can presume that the possible formation mechanism of the tribofilm in these composites is triggered by the transfer of a third body particle from the steel ball at the junction of the tribo-pairs, onto the composite surface during sliding. With the ongoing sliding, the third body wear debris will be fractured and refined to form a homogeneous mass that is essentially forced into the wear track under the applied load, leading to the formation of a tribofilm. This latter can cushion the load or fracture and serve as the source of wear debris.

4. Conclusion

TiC-Ni(Si, Ti) composites were successfully elaborated through pressureless sintering at 1080 °C for 4 h from pure Ni and Ti_3SiC_2 MAX phase (10, 20 and 30 wt.%) powders. The microstructural characterization, and mechanical and tribological behaviors of the composites have been investigated. From the totality of our results, the following conclusions can be drawn:

1. After sintering, Ti_3SiC_2 MAX phase was totally decomposed and transformed to TiC phase. Meanwhile, the de-intercalated Si and Ti atoms diffuse into Ni matrix giving a rise of Ni(Si, Ti) solid solution.
2. The hardness of NTSC composites increased linearly as a function of Ti_3SiC_2 content up to 20 wt.%. NTSC20 composite is $\sim$ 2.5 times harder than pure Ni. The improvement of hardness was attributed to the in situ formation of hard TiC particles, Ni(Si, Ti) solid solution formation and the good bonding between TiC and Ni(Si, Ti) matrix.
3. TiC content within the composites has no significant effect on the friction coefficient (μ) values under the applied loads; it varies between $\sim$ 0.50 and $\sim$ 0.75.
4. All TiC-Ni(Si, Ti) composites exhibited better wear resistance than Ni. Under 6 N load, the wear rate (WR) values were 20.42×10^{-5} mm^3/N m and 0.64×10^{-5} mm^3/N m for pure Ni and NTSC20 composite, respectively. SEM and Raman spectroscopy studies on the worn surfaces of the elaborated composites under all applied loads revealed the presence of a lubricious tribofilms, composed of Fe_3O_4 and α-Fe_2O_3 iron oxides.

Acknowledgments

The authors would like to thank Mme Zedouri and all staff working at ENSMM Annaba (Algeria) for the sliding experiments and Mr. Amine Soualili for conducting SEM analysis at CRTI research center (Research Center in Industrial Technologies, Cheraga, Algeria). This research did not receive any specific grant from funding agencies in the public, commercial or not-for-profit sectors.

References

1. C.S. Ramesh, S.K. Seshadri, and K.J.L. Iyer, Wear Resistance of Nickel-Fly Ash Composite Coatings, *Wear*, 1991, **145**, p 189–195
2. C.S. Ramesh and S.K. Seshadri, Tribological Characteristics of Nickel Based Composite Coatings, *Wear*, 2003, **255**, p 893–902
3. C. Cui, Z. Guo, H. Wang, and J. Hu, In situ TiC Particles Reinforced Grey Cast Iron Composite Fabricated by Laser Cladding of Ni-Ti-C System, *J. Mater. Proc. Technol.*, 2007, **183**, p 380–385
4. A. Gaard, P. Krakhmalev, and J. Bergström, Microstructural Characterization and Wear Behavior of (Fe, Ni)-TiC MMC Prepared by DMLS, *J. Alloys Compd.*, 2006, **421**, p 166–171
5. F. Akhtarab and S.J. Guoa, Microstructure, Mechanical and Fretting Wear Properties of TiC-Stainless Steel Composites, *Mater. Charact.*, 2008, **59**, p 84–90
6. Y. Pachaury and Y.C. Shin, Assessment of Sub-Surface Damage During Machining of Additively Manufactured Fe-TiC Metal Matrix Composites, *J. Mater. Proc. Technol.*, 2019, **266**, p 173–183
7. A. Benamor, Y. Hadji, N. Chiker, A. Haddad, B. Guedouar, M. Labaiz, M. Hakem, A. Tricoteaux, C. Nivot, J.P. Erauw, R. Badji, and M. Hadji, Spark Plasma Sintering and Tribological Behavior of Ti_3SiC_2-Ti_5Si_3-TiC Composites, Ceram. Inter., 2019, (**in printing**)
8. N.H. Loh, S.B. Tor, and K.A. Khor, Production of Metal Matrix Composite Part by Powder Injection Molding, *J. Mater. Proc. Technol.*, 2001, **108**, p 398–407
9. M. Niu, Q. Bi, L. Kong, J. Yang, and W. Liu, A Study of Ni_3Si-Based Composite Coating Fabricated by Self-Propagating High Temperature Synthesis Casting Route, *Surf. Coat. Technol.*, 2011, **205**, p 4249–4253
10. M. Niu, Q. Bi, S. Zhu, J. Yang, and W. Liu, Microstructure, Phase Transition and Tribological Performances of Ni_3Si-Based Self-Lubricating Composite Coatings, *J. Alloys Compd.*, 2013, **555**, p 367–374
11. L. Wenhu and T. Ling, Study on Microstructure and Properties of TiC-Ni_3Si/Ni Based Composite Coating by Arc Welding, *Hot Work. Technol.*, 2011, **16**, p 137
12. M.W. Barsoum, The $M_{n+1}AX_n$ Phases: A New Class of Solids; Thermodynamically Stable Nanolaminates, *Prog. Solid State Chem.*, 2000, **28**, p 201–281

13. M.W. Barsoum and M. Radovic, Elastic and Mechanical Properties of the MAX Phases, *Annu. Rev. Mater. Res.*, 2011, **41**, p 195–227
14. E.I. Istomina, P.V. Istomin, and A.V. Nadutkin, Preparation of Ti_3SiC_2 through Reduction of Titanium Dioxide with Silicon Carbide, *Inorg. Mater.*, 2016, **52**, p 134–135
15. T. El-Raghy and M.W. Barsoum, Diffusion Kinetics of the Carburization and Silicidation of Ti_3SiC_2, *J. Appl. Phys.*, 1998, **83**, p 112
16. N. Chiker, A. Haddad, Y. Hadji, M.E.A. Benammar, M. Azzaz, M. Yahi, M. Hadji, M.W. Barsoum, and T. Sahraoui, Infiltration Behavior of Cu and Ti fillers into Ti_2AlC/Ti_3AlC_2 Composites During Tungsten Inert Gas (TIG)brazing, *Ceram. Int.*, 2018, **44**, p 3282–3290
17. W. Wang, H. Zhai, L. Chen, Z. Huang, C. Baumgärtner, P. Greil, and G. Bei, Preparation and Mechanical Properties of In Situ TiC_x-Ni (Si, Ti) Alloy Composites, *Mater. Sci. Eng. A*, 2014, **616**, p 214–218
18. L. Lutterotti, MAUD: Material Analysis Using Di-raction. Program Download, Mirrored at CCP14; 1997–2009
19. L. Lutterotti, S. Matthies, and H.-R. Wenk, MAUD: A Friendly Java Program for Material Analysis Using Di-raction, *IUCr CPD Newsl.*, 1999, **21**, p 14
20. Y. Hadji, A. Tricoteaux, M.G. Ben Ghorbal, M. Yahi, R. Badji, T. Sahraoui, M. Hadji, and M.W. Barsoum, Microstructure and Microindentation of Ti_3SiC_2-Titanium Filler Brazed Joints by Tungsten Inert Gas (TIG) Process, *Ceram. Int.*, 2017, **43**, p 7284–7290
21. M. Leonhardt, W. Löser, and H.G. Lindenkreuz, Metastable Phase Formation in Undercooled Eutectic Ni78.6Si21.4 Melts, *Mater. Sci. Eng. A*, 1999, **271**, p 31–37
22. L. Ca, R.F. Cochrane, and A.M. Mullis, Microstructural Evolution and Phase Formation in Rapidly Solidified Ni-25.3 at.% Si Alloy, *Metall. Mater. Trans. A*, 2015, **46**, p 705–4715
23. J. Xu, G. Chen, Z. Zhang, M. Meng, Y. Zhao, X. Liu, X. Zhou, Q. Yan, and Z. Zhang, Microstructure and Mechanical Properties of In situ α-Al2O3p/Al-12Si Composites Fabricated by Direct Melt Reaction Method with Aid of Electromagnetic Stirring, *Mater. Res. Express.*, 2018, **5**, p 116502
24. S. Gupta, T. Hammann, R. Johnson, and M.F. Riyad, Synthesis and Characterization of Novel Al-Matrix Composites Reinforced with Ti_3SiC_2 Particulates, *J. Mater. Eng. Perform.*, 2015, **24**, p 1011–1017
25. Y.S. Zhang, Z. Han, K. Wang, and K. Lu, Friction and Wear Behaviors of Nanocrystalline Surface Layer of Pure Copper, *Wear*, 2006, **260**, p 942–948
26. C.S. Ramesh, R.N. Ahmed, M.A. Mujeebu, and M.Z. Abdullah, Development and Performance Analysis of Novel Cast Copper-SiC-Gr Hybrid Composites, *Mater. Des.*, 2009, **30**, p 1957–1965
27. N. Saka and D.P. Karalekas, Friction and wear of particle reinforced metal ceramic composites, in: K.C. Ludema (Ed.), Proceedings of the Conference on Wear of Materials, ASME, New York, (1985) pp. 784–793
28. E.R.I. Mahmoud, M. Takahash, T. Shibayanagi, and K. Ikeuchi, Wear Characteristics of Surface Hybrid-MMCs Layer Fabricated on Aluminum Plate by Friction Stir Processing, *Wear*, 2010, **268**, p 1111–1121
29. B.V.M. Kumar, B. Basu, J. Vizintin, and M. Kalin, Tribochemistry in Sliding Wear of TiCN-Ni-Based Cermets, *J. Mater. Res.*, 2008, **23**, p 1214–1227
30. T.L. Stewart and K.P. Plucknett, The Sliding Wear of TiC and Ti(C, N) Cermets Prepared with a Stoichiometric Ni3Al Binder, *Wear*, 2014, **318**, p 153–167
31. D.L.A. de Faria, S.V. de Silva, and M.T. Oliveira, Raman Microspectroscopy of Some Iron Oxides Raman and Oxyhydroxides, *J. Raman Spectrosc.*, 1997, **28**, p 873–878
32. O.N. Shebanova and P. Lazor, Raman Spectroscopic Study of Magnetite (FeFe2O4): A New Assignment for the Vibrational Spectrum, *J. Solid State Chem.*, 2003, **174**, p 424–430
33. K.S.K. Varadwaj, M.J. Panigrahi, and J. Ghose, Effect of Capping and Particle Size on Raman Laser-Induced Degradation of γ-Fe_2O_3 Nanoparticles, *J. Solid State Chem.*, 2004, **177**, p 4286–4292
34. Z.S. Hu, J.X. Dong, and G.X. Chen, Study on Antiwear and Reducing Friction Additive of Nanometer Ferric Oxide, *Tribol. Int.*, 1998, **31**, p 355–360
35. L. Xiang, C. Gao, Y. Wang, Z. Pan, and D. Hu, Tribological and Tribochemical Properties of Magnetite Nanoflakes as Additives in Oil Lubricants, *Particuology*, 2013, **17**, p 136–144
36. R. Ramadoss, N. Kumar, R. Pandian, S. Dash, T.R. Ravindran, D. Arivuoli, and A.K. Tyagi, Tribological Properties and Deformation Mechanism of TiAlN Coating sliding with Various Counterbodies, *Tribol. Int.*, 2013, **66**, p 143–149
37. A.K. Srivastava and K. Das, The Abrasive Wear Resistance of TiC and (Ti, W)C-Reinforced Fe-17Mn Austenitic Steel Matrix Composites, *Tribol. Int.*, 2010, **43**, p 944–950
38. I. Çelikyürek, N.Ö. Körpe, T. Ölçer, and R. Gürler, Microstructure, Properties and Wear Behaviors of $(Ni_3Al)_p$ Reinforced Cu Matrix Composites, *J. Mater. Sci. Technol.*, 2011, **27**, p 937–943
39. V.G.B. Kumar, C.S.P. Rao, and N. Selvaraj, Studies on Mechanical and Dry Sliding Wear of Al6061-SiC Composites, *Compos. Part B Eng.*, 2012, **43**, p 1185–1191